

SUPPLEMENTARY MATERIAL

Characteristics of Size Distributions at Urban and Rural Locations in New York

Min-Suk Bae¹, James J. Schwab¹, Olga Hogrefe¹, Brian P. Frank², G. Garland Lala¹, Kenneth L. Demerjian¹

1 Atmospheric Sciences Research Center, University at Albany, State University of New York, Albany, New York, USA

2 Division of Air Resources, New York State Department of Environmental Conservation, Albany, NY, USA

Diffusion Loss Correction for the Sampling Lines

Fig. S-1 shows the diffusion losses for the sampling lines for the Nano SMPS and LDMA SMPS. When the Nano SMPS was set up with a 5.0 l/min bypass flow for WFM02 the integrated total average of the diffusion losses for the sampling lines was less than 2%, so these diffusion losses in the sampling lines are almost negligible for total aerosol nano particle number concentrations. However, since the diffusion losses are size dependent (the smaller the particle the more susceptible it is to diffusion), these losses cannot be ignored when measuring very small aerosols.

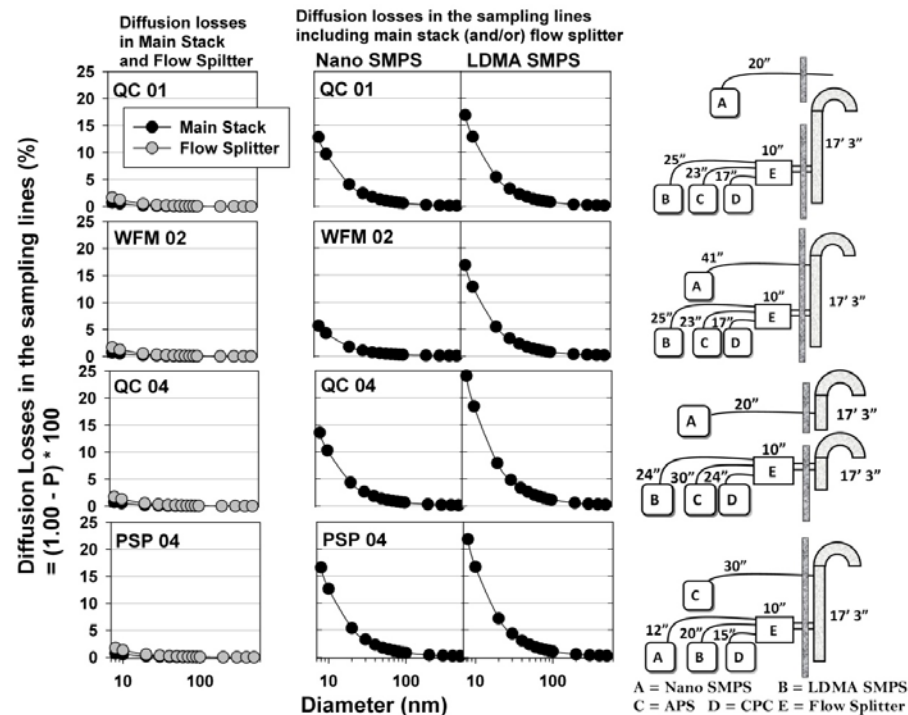


Fig. S-1. Computed diffusion losses (%) for the Nano and LDMA SMPS sampling lines. The left panels only show the diffusion losses in Main Stack and Flow Splitter. The center panels show the diffusion losses in the sampling lines including main stack (and/or) flow splitter. The right panels show the schematic diagrams for the setup related to campaigns.

(Note: Total flow rate of Nano SMPS for the WFM02 campaign includes 5.0 lpm bypass)

Diffusion Loss Correction for the SMPS

Originally all data was analyzed after the four measurement campaigns using TSI software available at that time, which did not include the diffusion correction option. The applications of the diffusion correction on the data sets are presented below, but unless otherwise noted, all data used has been recalculated with the updated software (Aerosol Instrument Manager Software Version 8.0) to compensate for diffusion losses (in addition to the standard multiple charging correction).

Recovery of an aerosol size distribution from particle counts recorded during SMPS measurements can be described in terms of the instrument function relating reported raw counts to concentrations, which operationally produces the reported number of particles in a given bin (dN) from the raw number of particle counts measured by the CPC (dC). That is, this function is given by dN/dC , or more precisely as $\Delta N/\Delta C$. In Fig. S-2 we present this function with and without the diffusion correction for the SMPS, and the diffusion correction factors themselves (the standard multiple charging correction is always applied). These quantities in Fig. S-2 are computed for two periods encompassing 10 size distributions for each campaign. (For the QC campaigns, a size distribution is derived from a single 2.5 minute SMPS scan, while for the WFM and PSP campaigns two 2.5 minute SMPS scans are averaged to derive each size distribution.) The periods were chosen to represent moderate to high number concentrations (cm^{-3}) for the campaign, and to explore possible sensitivity of the correction to varying concentrations and particle distributions.

For our conditions, the diffusion correction is 12-15% at 100nm, increases to about a factor of two at 20 nm, then increases rapidly with decreasing diameter, reaching values at the lowest reported mobility diameters of almost eight for SMPS flow of 0.3 lpm and between four and five for SMPS flow of 0.6 lpm. The rapidly increasing diffusion correction presents a dilemma for those trying to obtain size distributions for particles down to very small sizes. Clearly the correction is necessary to produce reliable data for sizes on the order of 20 nm or smaller. However, applying the correction to the very smallest size bins in our campaigns (below 8 nm in our campaigns) produced sporadic and noisy data. This is because the diffusion correction, and by extension the $(\Delta N/\Delta C)$ becomes so large (as big as 20,000 - 30,000) that single counts in the smallest size bins become significantly over emphasized resulting in unrealistic particle size distributions. We compromised by only considering sizes above 8 nm, which unfortunately required excluding data for smaller size bins.

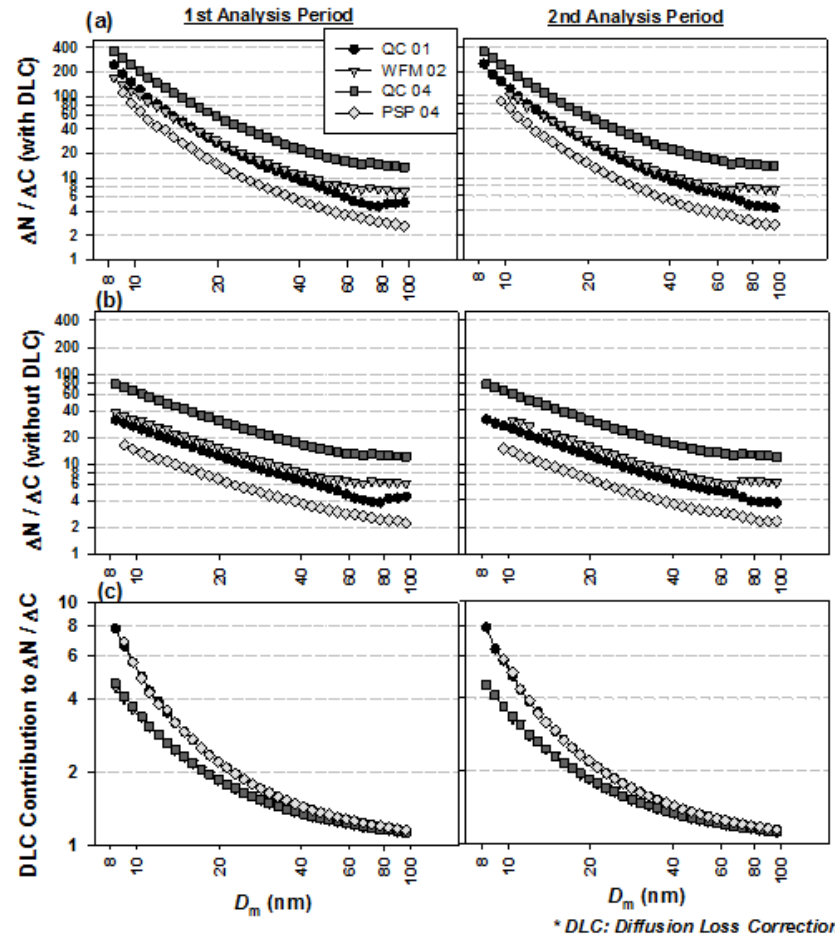


Fig. S-2. The function $\Delta N/\Delta C$ for the Nano SMPS in each of the four measurement campaigns. Panel (a) shows $\Delta N/\Delta C$ with the diffusion loss correction included, panel (b) shows $\Delta N/\Delta C$ without the diffusion loss correction, and panel (c) shows the contribution of the diffusion loss correction to $\Delta N/\Delta C$.

Particle Growth Events at the Rural Site

During the measurement periods at the rural sites one very strong particle formation and growth event with very high concentrations down to the smallest reported diameter of 8nm was observed for each site. Figure S-3 shows the details of these growth events over a 3 day period for these two events.

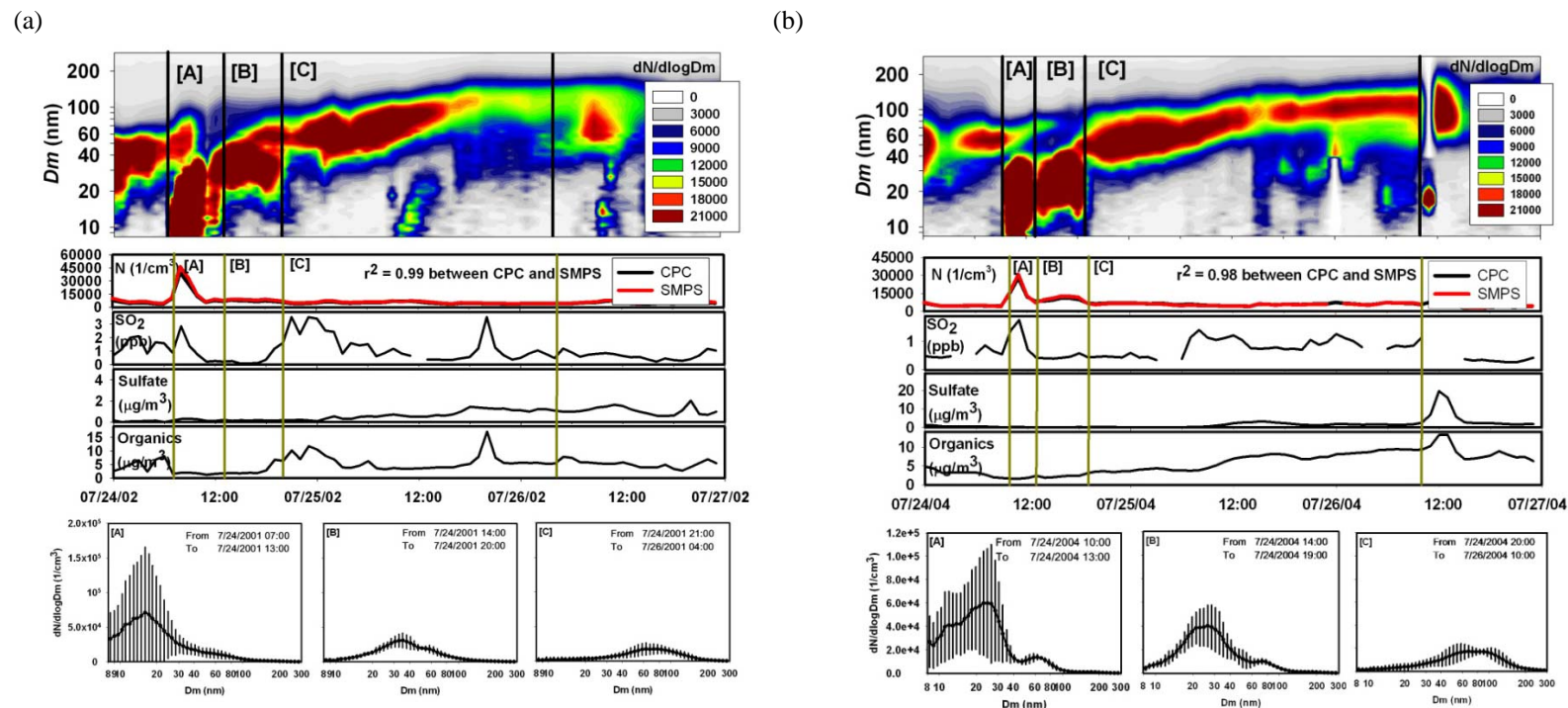


Fig. S-3. Evolution of particle size distributions and particle concentrations ($dN/d\log D_m$) ($1/cm^3$), time series traces for the hourly number concentration ($1/cm^3$) measured by the CPC (dark yellow line) & SMPS (8.35 – 283.9 nm) (red), as well as SO_2 , Sulfate, and Organics during the particle growth events for the (a) WFM 02 and the (b) PSP 04 campaigns. These events have been classified into three consecutive periods (A, B, and C) based on the dynamics of number concentrations. The particle size distributions changed considerably during this event.

We have divided the growth events into three consecutive periods (A, B, and C) based on the dynamics of number concentrations (the letters correspond to early, middle and late in the growth event). As the bottom panels of Fig. S-3 show, the size distributions of number concentrations changed considerably from period A to periods B and then C. The increase in SO₂ coincides with the large increase in particle concentration. For these events, there are no increases in CO, NO, and NO₂ levels. Particle acidity was examined based on the ratio of measured molar ammonium concentrations (multiplied by two) to the measured molar sulfate concentration. A ratio equal to one suggests that sulfate might be fully neutralized by ammonium in the form of (NH₄)₂SO₄. On the basis of this definition, ultrafine particles appeared to be neutralized before and during the initial stages of the growth and to become more acidic as the event grew into the late stages. For these new particle formation and growth events, we believe two important processes contribute to the observed behavior.

First, the association with observed SO₂ strongly suggests formation of new sulfate particles. Number concentrations of particles below 10 nm were significantly associated with SO₂ during the event. Photochemical reactions oxidizing SO₂ to sulfuric acid and its subsequent nucleation with water and possibly ammonia appear to be primarily responsible for the strong growth event. Many research papers have observed this type of nucleation event with a characteristic banana shape (Jeong, et al., 2006; Watson, et al., 2006; Zhang, et al., 2005). The appearance of our under 10 nm size measurements in this study is somewhat different from the prior studies, which may suggest that we need to consider further possibilities. The associated surface wind direction and wind speed are shown in Figure S-4 as hourly vectors. The wind speed is found to increase after initial stage without significant direction changes lending support to the idea that this is a regional particle formation event. In addition, 1-day backward trajectories were calculated using the hybrid single-particle Lagrangian integrated trajectories (HYSPPLIT 4.5) model, with the meteorological data from the EDAS data set, to examine the origins of air parcels arriving at the sampling site (77.21 W, 42.09 N) for the July 24, 2004 at 10:00 am. Figure S-4 presents these 24 hour backward trajectories at elevations of 2, 267, & 517 m (above the sampling site ground level) with updates every 6 hour. Based on the trajectories, nucleation days were influenced primarily by the clean air mass from the north that had been transported to the PSP and WFM sampling sites, cleaning the air and setting the stage for fresh sulfate particle production.

Second, the events occurred well after sunrise and at times that are consistent with the breakdown of the nocturnal boundary layer and mixing down of air from aloft. Notice the changes in elevation of the trajectories, and the increase in T and decrease in RH that accompany the rapid increase in N (< 10nm). The mixing mechanism merits further exploration that would benefit from more detailed summertime upper-air measurements (Nilsson and Kulmala, 1998; Watson, et al., 2006). We think it likely that both of these processes contribute to the strong growth events we observed.

Meteorological Conditions and Back Trajectories for Particle Growth Events at the Rural Site

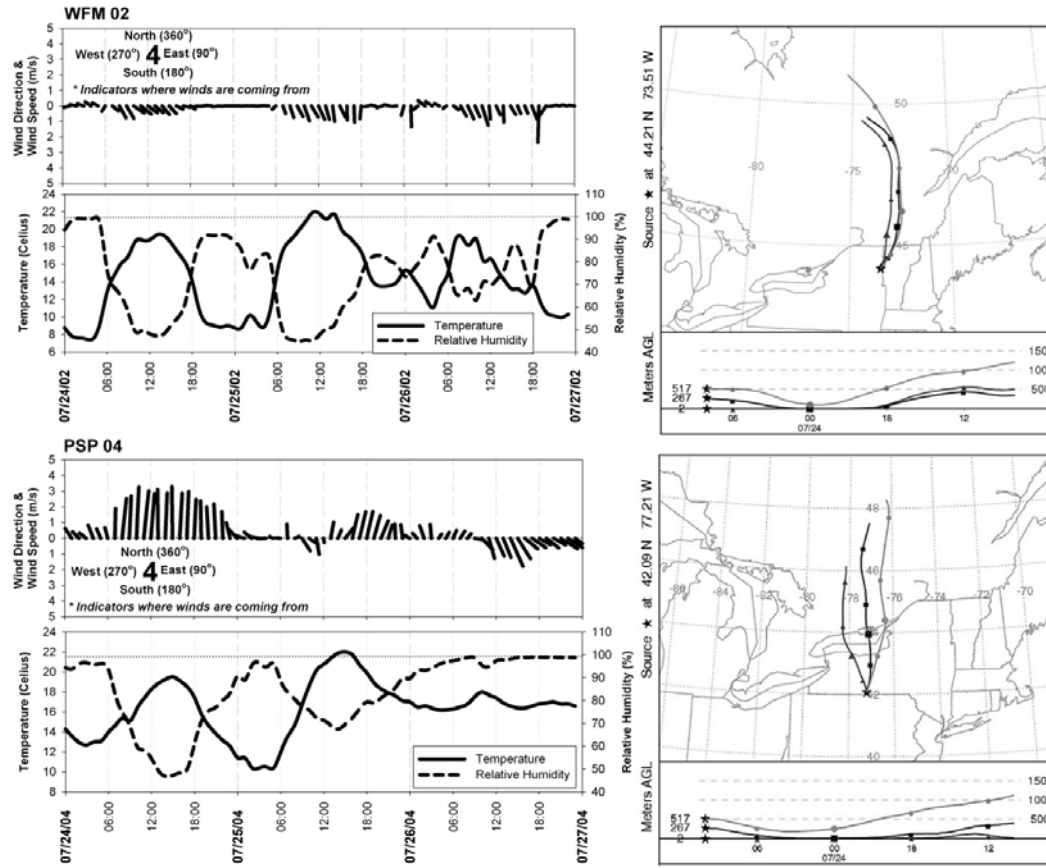


Fig. S-4. The wind direction, wind speed (the vector length represents the wind speed and the vector direction shows the wind direction, where 0°, 90°, 180°, 270° represent north, east, south, and west, respectively), temperature (Celsius), and relative humidity (RH). The hybrid single-particle Lagrangian integrated trajectories (HYSPPLIT 4.5) model at the sampling sites on July 24 at 10:00 AM in 2004 and on July 24 at 8:00 AM in 2002 (24 h backward trajectories with elevations of 2, 267, 517 m (above the sampling site level) indicated by every 6 h).

Particle Growth Rate

The overall growth rates are indicated as a slope of 2.8 nm and 2.4 nm per hour for WFM 02 and PSP 04, respectively.

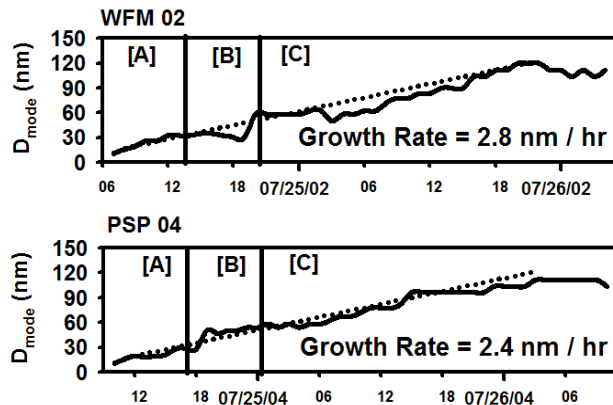


Fig. S-5. Growth rate calculated using the time evolution of the mode diameter (D_{mode}) of the particle size distribution.

Figure S-5 illustrates the method used to calculate the growth rates for the two strong particle formation and growth events discussed in the paper and the section above. The growth rate is calculated as the slope of the linear fit to the mode diameter versus time. It can be seen from this figure that in these two cases the particle growth continued for roughly 36 hours.

Periods of high particle concentration at the urban site

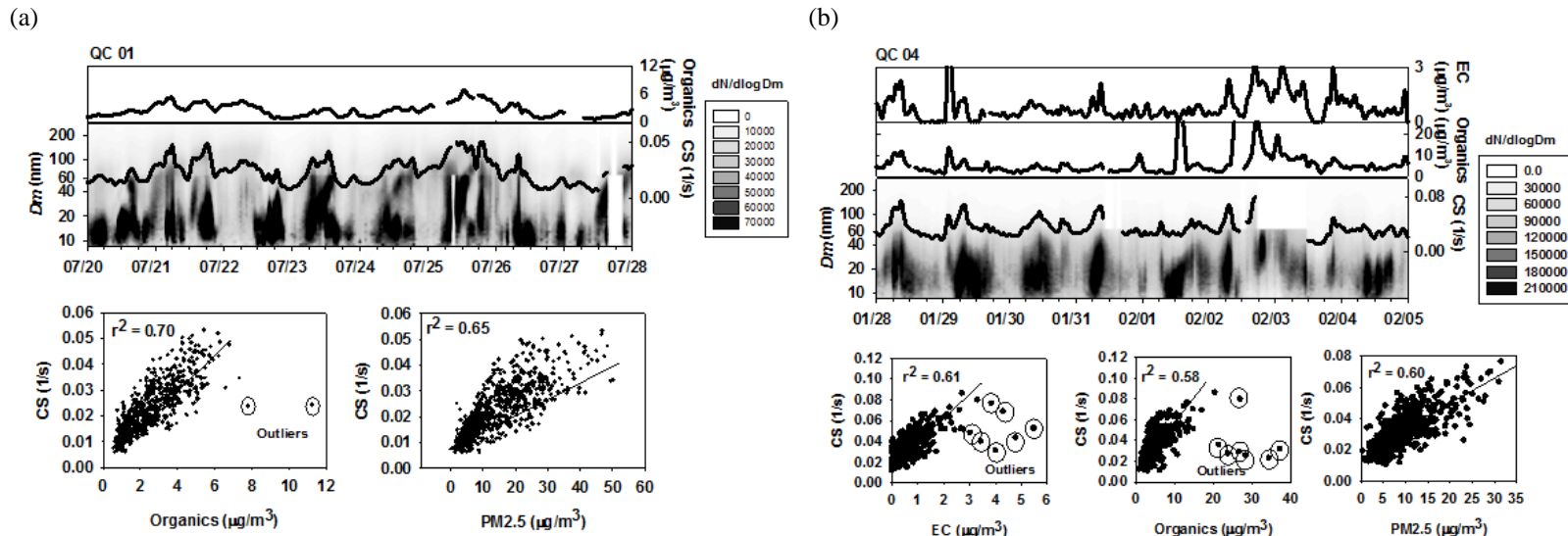


Fig. S-6. Evolution of particle size distributions and particle concentrations ($dN/d\log D_m$) (1/cm³), time series traces for the hourly condensation sink (CS), Elemental Carbon (EC) and Organics during selected periods for the QC 01 and the QC 04 campaigns.

Figure S-6 shows data for eight days of measurements for the QC01 and QC04 campaigns. There are periods of high particle concentration essentially every day, but they do vary in peak concentration, duration, and timing. The pattern is more regular in the winter, when the boundary layer is lower, but changes in temperature and winds influence distributions during that period as well. The lower panels show the relatively strong relationships between the condensation sink and the PM_{2.5} mass, PM organics, and PM EC for these periods, indicating once again the dominating influence of carbonaceous emissions to particle growth at the urban site.

References

- Jeong, C.-H. , Evans, G.J., Hopke, P.K., Chalupa, D., and Utell, M.: Influence of Atmospheric Dispersion and New Particle Formation Events on Ambient Particle Number Concentration in Rochester, United States, and Toronto, Canada, *J. Air Waste Manage. Assoc.*, 56, 431-443, 2006.
- Nilsson, E. D., and Kulmala, M.: The potential for atmospheric mixing processes to enhance the binary nucleation rate, *J. Geophys. Res.*, 103, 1381-1389, 1998.
- Watson, J. G., Chow, J. C., Park, K., and Lowenthal, D. H.: Nanoparticle and Ultrafine Particle Events at the Fresno Supersite, *J. Air Waste Manage. Assoc.*, 56, 417-430, 2006.
- Zhang, Q., Canagaratna, M., Jayne, J. T., Worsnop, D. R., and Jimenez, J.-L.: Time- and Size-resolved Chemical Composition of Submicron Particles in Pittsburgh: Implications for Aerosol Sources and Processes, *J. Geophys. Res.*, 110, D07S09, doi:10.1029/2004JD004649, 2005.